Supporting Information

Nitric Oxide-Enhanced Blood-Brain Barrier Penetration and Mitochondria-Targeted Antioxidant Carbon Dots for Alzheimer's Disease

Materials

Dulbecco's Modified Eagle Medium (DMEM) and DMEM/Ham's F-12 (DMEM/F12) were obtained from Hyclone (Singapore). Fetal bovine serum (FBS) was purchased from Gibco (Singapore). Phosphate-buffered saline (PBS), Cell Counting Kit-8 (CCK-8), penicillin–streptomycin solution, trypsin–EDTA solution, anhydrous ethanol, DAF-FM DA (NO fluorescence probe), L-NAME (eNOS inhibitor), Mitochondrial Membrane Potential Detection Kit (JC-1) and a reactive oxygen species (ROS) detection kit were obtained from Beyotime (Shanghai, China).Epigallocatechin gallate (EGCG, ≥96%), m-phenylenediamine (m-PD, ≥99%), L-arginine (L-Arg, ≥99%), Fibronectin (0.2 mg/mL), Transwell Inserts, 1,1,1,3,3,3-hexafluoro-2-propanol (HFIP), 5-Fluoro-2'-deoxyuridine (FUDR) and fluorescein isothiocyanate (FITC) were purchased from Macklin Biochemical Co., Ltd. (Shanghai, China). Thioflavin T (ThT) and MitoSOX was obtained from MedChemExpress (MCE, USA). Human neuroblastoma SH-SY5Y cells were purchased from the Cell Bank of the Chinese Academy of Sciences (Shanghai, China). ZO-1 Rabbit mAb and MMP9 Rabbit mAb were purchased from Huidan Biotechnology Co., Ltd. (Hangzhou, China). DyLight 488 goat anti-rabbit IgG and DyLight 594 goat anti-rabbit IgG were obtained from Bioss Biotechnology Co., Ltd. (Wuhan, China). Normal goat serum (blocking solution) and Triton X-100 were purchased from Servicebio (Wuhan, China).

Instruments and characterization

The morphology and size distribution of EMA-CDs were characterized using high-resolution transmission electron microscopy (HR-TEM, JEM-2100F, JEOL Ltd., Japan). The elemental composition was analyzed by X-ray photoelectron spectroscopy (XPS, ESCALAB 250Xi, Thermo Fisher Scientific, USA). Surface functional groups were identified by Fourier transform infrared spectroscopy (FTIR, Tensor 27, Bruker Optik GmbH, Germany). UV–Vis absorption spectra were recorded using a UV–Vis spectrophotometer (UV-8000A, Metash Instruments Co., Ltd., China), and the fluorescence properties were analyzed using a steady-state and time-resolved fluorescence spectrometer (FLS980, Edinburgh Instruments Ltd.,

UK).For biological evaluation, cellular imaging was performed using a fluorescence microscope (DM3000, Leica Microsystems, China). Cell viability was assessed using the CCK-8 assay, and optical density (OD) values were determined with a microplate reader (Multiskan FC, Thermo Fisher Scientific, China).

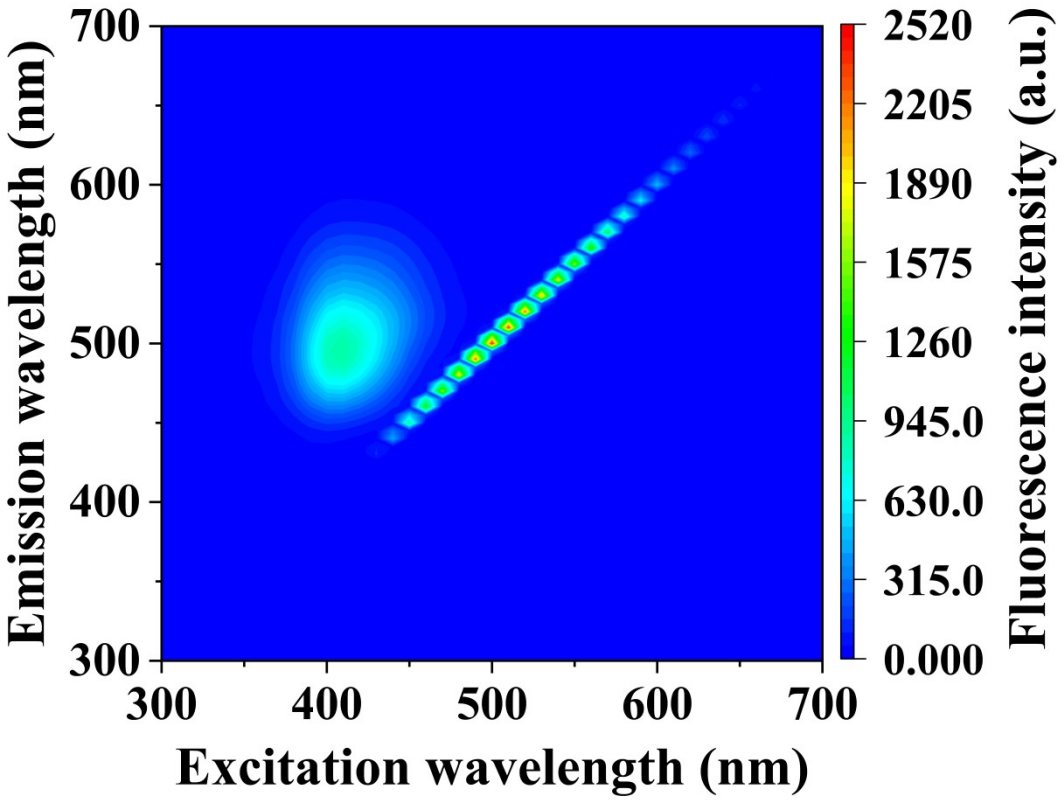

Fig. S1. 3D excitation-emission matrix fluorescence spectrum.

Cell viability assay

SH-SY5Y and bEnd.3 cells were seeded in 24-well plates at a density of 1×10^5 cells per well and incubated for 24 h to allow adhesion. Subsequently, the cells were treated with EMA-CDs at a concentration of 500 μg/mL in complete medium for 1 h. After treatment, the cells were washed twice with PBS and fixed with formaldehyd.

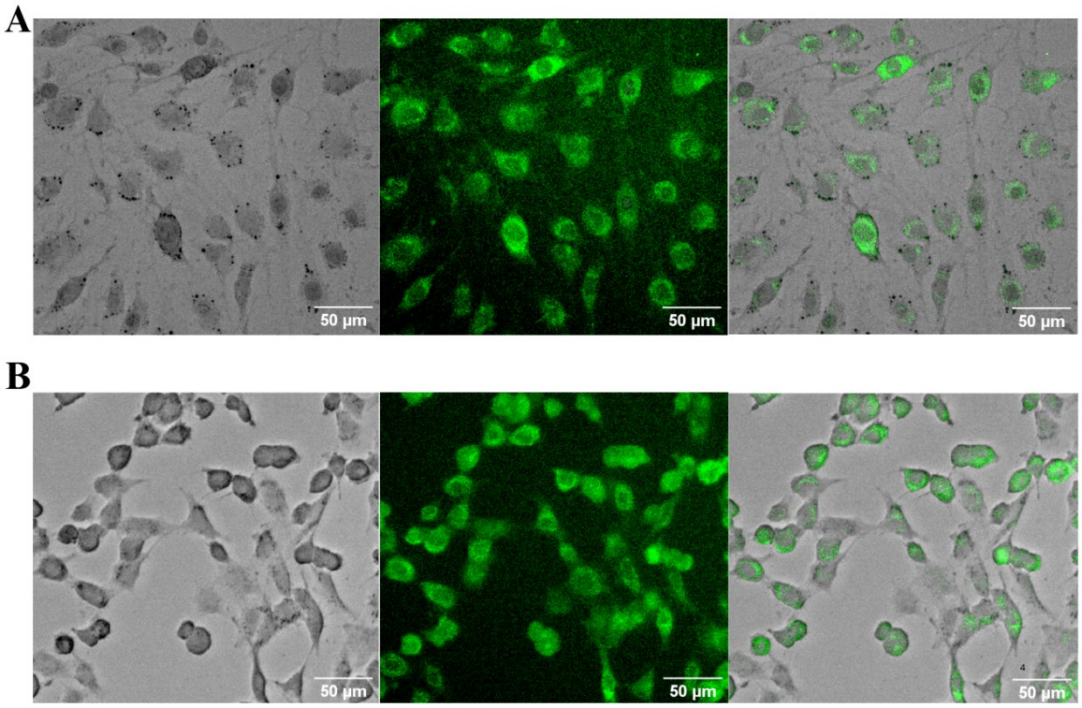

Fig. S2. Fluorescence imagings of (A) bEnd.3 cells and (B) SH-SY5Y cells treated with EMA-CDs.

FITC Labeling of EMA-CDs

To enhance the fluorescence intensity of EMA-CDs for colocalization experiments, fluorescein isothiocyanate (FITC) was used to label EMA-CDs, yielding EMA-CDs–FITC. Briefly, 5.0 mg of FITC was dissolved in 2 mL of deionized water and mixed with 10 mL of EMA-CDs solution (1 mg/mL) under continuous stirring at room temperature. The pH of the reaction system was carefully maintained between 7.2 and 7.4 to ensure optimal labeling efficiency. The mixture was wrapped in aluminum foil to protect it from light and stirred overnight to prevent dye photobleaching.After the reaction, the mixture was transferred into a dialysis bag (molecular weight cutoff: 3500 Da) and dialyzed against ultrapure water at 4 °C in the dark for 72 h to remove unbound FITC. The resulting EMA-CDs–FITC solution was collected. The successful conjugation of FITC onto the surface of EMA-CDs was confirmed by comparing the UV-Vis absorption spectra before and after labeling.

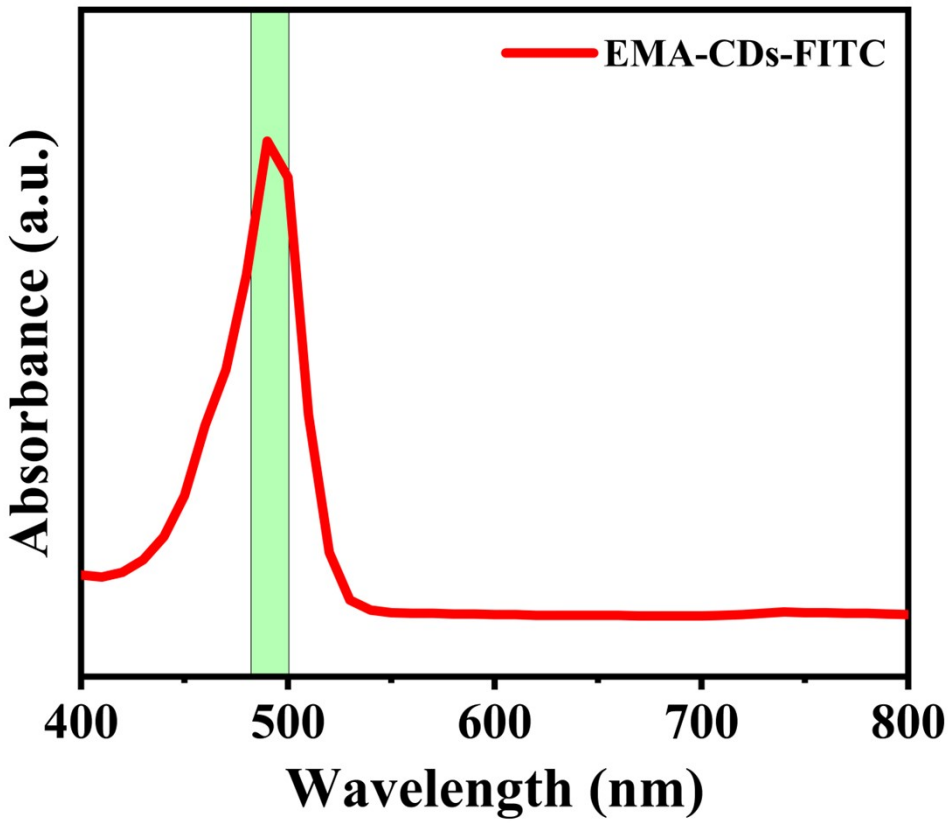

Fig. S3. UV-Visible absorption spectrum of EMA-CDs-FITC.

Free radical scavenging ability

ABTS Radical Scavenging Activity:7.4 mM ABTS and 2.6 mM potassium persulfate were mixed in equal volumes and reacted in the dark for 12 h to generate the $ABTS^{+}$• stock solution. This stock solution was then diluted until its absorbance at 734 nm was 0.70 ±0.02, yielding the working solution. For measurement, different concentrations of EMA-CDs were mixed with the working solution and reacted in the dark for 10 min. Absorbance was then measured at 734 nm.

DPPH radical scavenging activity: In the presence of EMA-CDs at different concentrations, we used a calibration curve of absorbance at 517 nm to determine the DPPH scavenging rate. Different concentrations of EMA-CDs were added to a DPPH ethanol solution (0.1 mM, 2 mL, pH = 7). The UV-visible absorbance at 517 nm was measured every 100 s over a 600-s period.

•OH radical scavenging activity：First, hydroxyl radicals are generated via the Fenton reaction, and then the scavenging effect of EMA-CDs on •OH radicals is evaluated by measuring the absorption peak of oxTMB at 652 nm. In summary, the reaction was conducted

in PBS buffer (0.01 M, pH 4.5), with the addition of H_2O_2 (100 mM), TMB (10 mM), and different concentrations of EMA-CDs (0 to 80 μg/mL), followed by a 5-min reaction. $FeSO_4$ (10 mM) was then added to generate •OH. The scavenging efficiency of •OH was calculated using the following formula: $[(A_2-A_1) / (A_2-A_0)] \times 100\%$, where A_0 is the absorbance of TMB alone, and A_1 and A_2 are the absorbances of oxTMB in the absence and presence of EMA-CDs, respectively.

•O_2^-scavenging activity：Using nitroblue tetrazolium chloride (NBT) as a probe, the scavenging efficiency of •O_2^- was determined. Riboflavin may undergo photoreduction in the presence of oxidants, and the reduced form is easily reoxidized under aerobic conditions, generating •O_2^-.This superoxide anion converts NBT into blue methanesulfonate, which has maximum absorption at 560 nm. The test solution typically consists of riboflavin (400 μM), methionine (260 mM), NBT (1.5 mM), and different concentrations (0 to 80 μg/mL) of EMA-CDs, along with PBS buffer (0.01 M, pH 7.4). The mixture was exposed to light for 300 s using a 30 W lamp. The absorption of methanethiol was quantified using a UV-visible spectrophotometer. The scavenging efficiency of •O_2^- was determined using the formula $[(A_1-A_2) / (A_1-A_0)] \times 100\%$,where A_0 represents the absorbance of NBT alone, and A_1 and A_2 represent the absorbance without and with EMA-CDs, respectively.

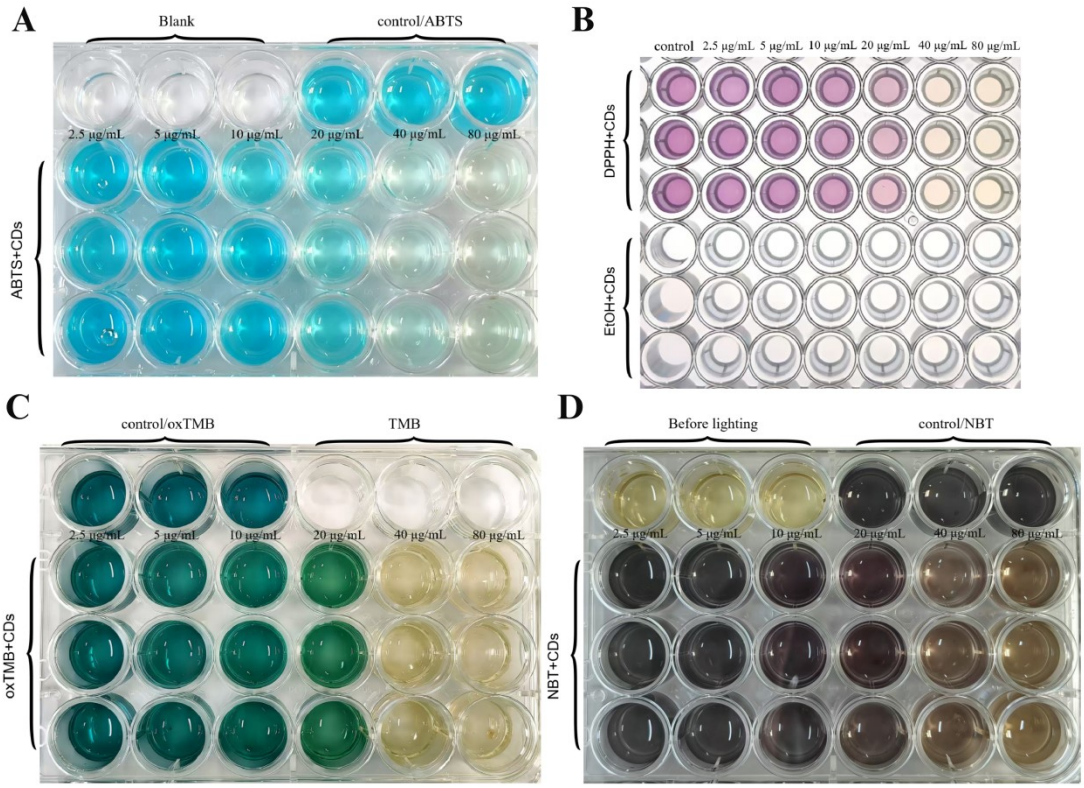

Fig. S4. Evaluation of the free radical scavenging activities of EMA-CDs at different concentrations (2.5-80 μg/mL), including (A) $ABTS^{+}$•, (B) DPPH, (C) •OH, and (D) $•O_2^-$ radicals.

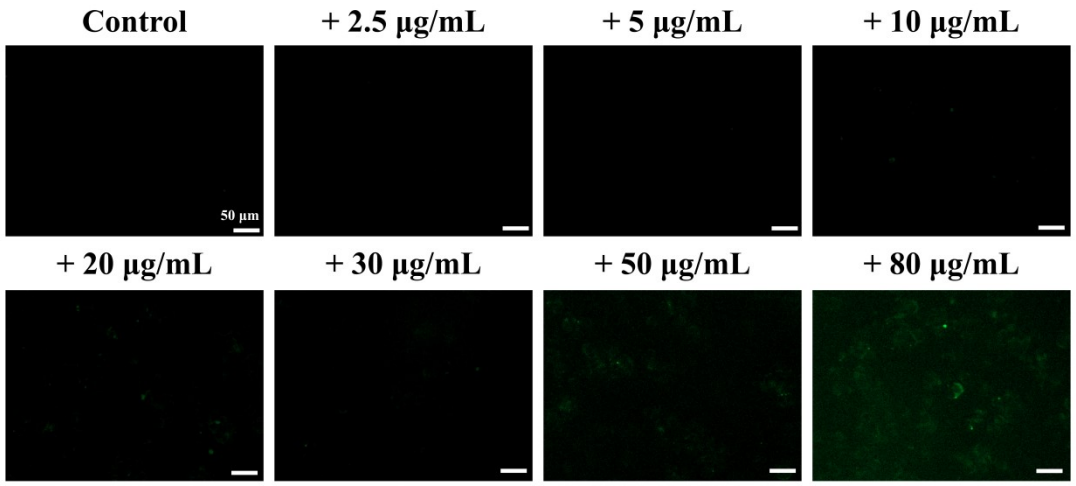

Fig. S5. Control group for the autofluorescence of EMA-CDs at the detection wavelength of DCFH-DA.

Verification of eNOS-Dependent NO Production

To verify that the promotion of NO generation by EMA-CDs is dependent on endothelial eNOS, an experiment utilizing the specific eNOS inhibitor L-NAME was performed. bEnd.3 cells were divided into three groups: a control group, an EMA-CDs-treated group, and an L-NAME+EMA-CDs co-treatment group. In the co-treatment group, cells were pre-incubated with 100 μg/mL L-NAME for 2 h to inhibit eNOS activity, followed by exposure to 80 μg/mL EMA-CDs. Intracellular NO levels in all groups were subsequently detected by incubation with the fluorescent probe DAF-FM DA for 20 min.

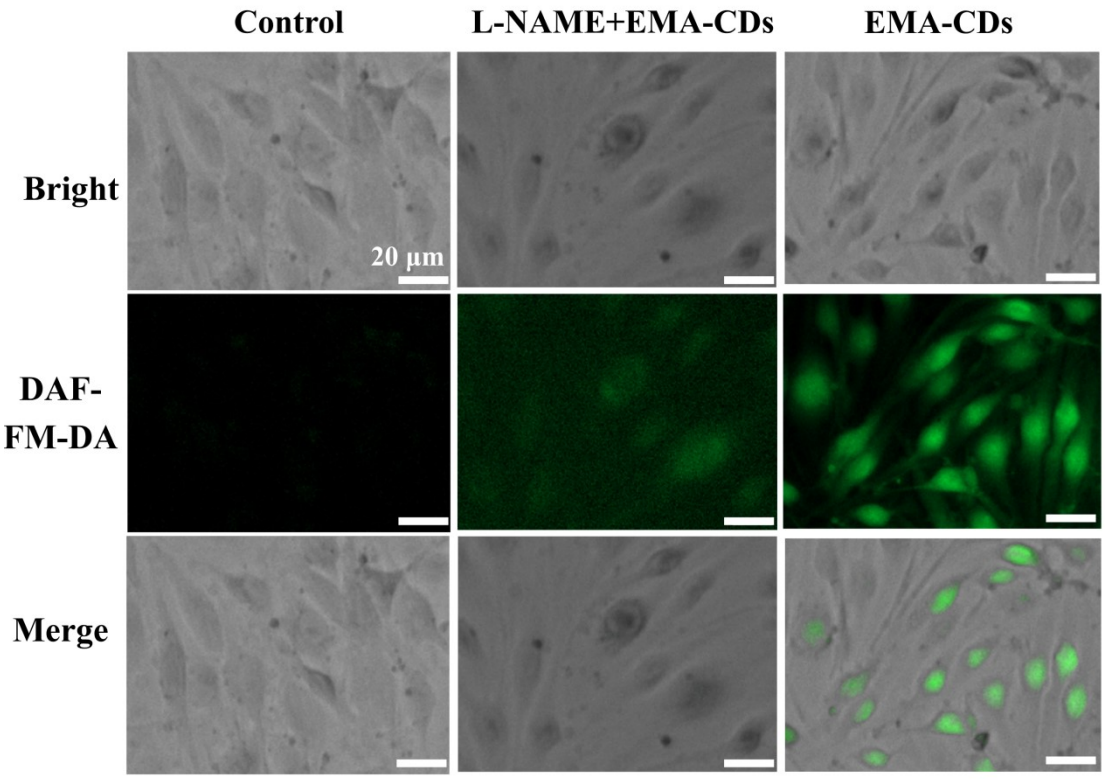

Fig. S6. Dependence of EMA-CD-induced NO generation on eNOS activity.

Tab. S1. A summary of the role of carbon dots in scavenging free radicals in the literature.

Name	Concentration (μg/mL)	$ABTS^{+}$• elimination (%)	DPPH elimination (%)	•OH elimination (%)	$•O_2^-$ elimination (%)	Reference
TNCDs	10	18	10			[1]
	20	39	17			
	40	71	28			
	80	96	41			
	120	99	63			
	200	100	81			
Ru-CDs	5	7	27			[2]
	20	17	56			
	40	25	67			
	60	30	72			
	80	41	80			
	100	50	80			
N-CDs	12.5	17	59	14		[3]
	25	39	72	43		
	50	62	81	75		
	100	97	90	93		
AA-CDs	5	10	8	18	23	[4]
	10	17	21	37	55	
	20	24	27	45	64	
	50	48	56	81	78	
	100	65	67	98	84	
	200	90	74	109	97	
CDs-1	35		38	4		[5]
	70		49	5		
	280		95	16		

CDs	200		22	41	26	[6]
	400		38	54	29	
	600		52	56	33	
	800		63	58	35	
	1000		76	65	43	
	2000		85	73	50	
LLC	15.625	5	82	50	21	[7]
	31.25	9	85	54	28	
	62.5	23	88	61	32	
	125	39	90	73	35	
	250	64	97	78	39	
	500	92	98	86	40	
	1000	98	99	93	43	
RA-CDs	25	35		11	6	[8]
	50	61		42	28	
	100	100		96	39	
CACDs	10		4	13	17	[9]
	25		16	31	54	
	50		48	36	72	
	100		66	74	79	
SeCDs	25		24	62	53	[10]
	50		36	73	76	
	100		48	77	86	
EMA-CDs	2.5	7	19	11	10	This work
	5	15	24	16	21	
	10	29	42	28	33	
	20	53	61	53	47	
	40	90	76	84	68	
	80	100	89	94	82	

Tab. S2. A summary of the role of carbon dots in inhibiting amyloid protein aggregation and depolymerizing amyloid fibrils in the literature.

Name	Amyloid	Amyloid concentration (μM)	Inhibitor concentration (μg/mL)	Inhibitory effect (%)	Disaggregation effect (%)	Reference
SeCDs	$A\beta_{42}$	20	10	51	47	[10]
SeCQDs	$A\beta_{40}$	100	5	37		[11]
			50	70		
OPCDs	$A\beta_{42}$	40	10	24		[12]
			20	30		
			50	60		
			100	80		
gCDs	$A\beta_{42}$	20	80	62.97	65	[13]
gCDs-E				90	76	
C-Dots	$A\beta_{42}$	10	2	16		[14]
			5	36		
			10	54		
CPDs	$A\beta_{40}$	25	1	19	30	[15]
			5	25	50	
			10	43	70	
			20	47	80	
			50	55	83	
			100	71	91	
75E-CPDs	$A\beta_{40}$	25	2.5	72	30	[16]
			5	78	40	
			10	83	62	
			20	91	75	
			40	97	90	
			80	99	92	
R-CD-75	$A\beta_{40}$	25	2	79	50	[17]
			5	81	70	
			10	97	80	
			20	92	87	
			50	99	95	

VP@RVG29	$A\beta_{42}$	25	80	73	69	[18]
NPs	$A\beta_{42}$	20	5	62	50	[19]
			10	70	65	
HSA-BFP@CDs	Aβ	25	10	57		[20]
			30	82		
			100	96		
CNDs	lysozyme	20	1	31	29	[21]
			5	58	46	
			10	82	58	
			25	93	61	
			50	94	61	
FA-LCDs	$A\beta_{42}$	20	100	90	95	[22]
EMA-CDs	$A\beta_{42}$	20	2.5	49	62	This work
			5	56	72	
			10	57	89	
			20	72	97	
			30	77	96	
			50	81	97	
			80	97	99	

[1] Warjurkar K, Patyal R, Sharma V. Sustainable Biomimetic Nanozymes: Catalase-Like Nitrogen-Doped Green Carbon Dots for Efficient Intracellular ROS Scavenging[J]. Advanced Sustainable Systems, 2026, 10(2): e01252. https://doi.org/10.1002/adsu.202501252.

[2] Patyal R, Warjurkar K, Sharma V. Optically Encoded Nanodots for Logic-Gated Sensing and Antioxidant Defense[J]. Langmuir, 2025, 41(44): 29801-29813. https://doi.org/10.1021/acs.langmuir.5c04249.

[3] Wang S, Chu K, Zhou X. Multifunctional red-luminescing carbon dots for pH sensing, antibacterial and antioxidant activities[J]. Journal of Molecular Structure, 2025: 144504. https://doi.org/10.1016/j.molstruc.2025.144504.

[4] Wang H, Sun S, Zhao Y, et al. Carbon dots with integrated photothermal antibacterial and heat-enhanced antioxidant properties for diabetic wound healing[J]. Small, 2024, 20(45): 2403160. https://doi.org/10.1002/smll.202403160.

[5] Li D, Wang X, Wang S, et al. Multifunctional carbon dots inhibit the amyloid fibrillation and scavenge free radicals[J]. Journal of Molecular Structure, 2025, 1326: 141134. https://doi.org/10.1016/j.molstruc.2024.141134.

[6] Wang H, Kang Y, Yang N, et al. Inhibition of UV-B stress in lettuce through enzyme-like Scutellaria baicalensis carbon dots[J]. Ecotoxicology and Environmental Safety, 2022, 246: 114177. https://doi.org/10.1016/j.ecoenv.2022.114177.

[7] Zheng Y, Liu J, Ma Y, et al. Calcined lotus leaf-derived carbon dots: enhanced hemostasis, anti-inflammatory, immunomodulatory properties for ulcerative colitis management[J]. Journal of Nanobiotechnology, 2026. https://doi.org/10.1186/s12951-026-04208-5.

[8] Xia J, Wang J, Liu F, et al. Red/NIR-I-Fluorescence Carbon Dots Based on Rhein with Active Oxygen Scavenging and Colitis Targeting for UC Therapeutics[J]. Advanced Healthcare Materials, 2024, 13(19): 2304674. https://doi.org/10.1002/adhm.202304674.

[9] Fan T, Cao X, Wang C, et al. Vitamin C derived carbon dots: inhibiting amyloid aggregation and scavenging reactive oxygen species[J]. New Journal of Chemistry, 2025, 49(2): 605-614. https://doi.org/10.1039/D4NJ03688C.

[10] Shao X, Fan T, Yan C, et al. Multifunctional selenium-doped carbon dots for modulating Alzheimer's disease related toxic ions, inhibiting amyloid aggregation and scavenging reactive oxygen species[J]. International Journal of Biological Macromolecules, 2025, 293: 139333. https://doi.org/10.1016/j.ijbiomac.2024.139333.

[11] Zhou X, Hu S, Wang S, et al. Large amino acid mimicking selenium-doped carbon quantum dots for multi-target therapy of Alzheimer's disease[J]. Frontiers in pharmacology, 2021, 12: 778613. https://doi.org/10.3389/fphar.2021.778613.

[12] Chung Y J, Lee B I, Park C B. Multifunctional carbon dots as a therapeutic nanoagent for modulating Cu (ii)-mediated β-amyloid aggregation[J]. Nanoscale, 2019, 11(13): 6297-6306. https://doi.org/10.1039/C9NR00473D.

[13] Yan C, Wang C, Shao X, et al. Dual-targeted carbon-dot-drugs nanoassemblies for

modulating Alzheimer's related amyloid-β aggregation and inhibiting fungal infection[J]. Materials Today Bio, 2021, 12: 100167. https://doi.org/10.1016/j.mtbio.2021.100167.

[14] X. Han, Z. Jing, W. Wu, et al. Biocompatible and blood-brain barrier permeable carbon dots for inhibition of Aβ fibrillation and toxicity, and BACE1 activity, Nanoscale 9(35) (2017) 12862-12866. https://doi.org/10.1039/C7NR04352J.

[15] Gao W, Wang W, Dong X, et al. Nitrogen-doped carbonized polymer dots: a potent scavenger and detector targeting Alzheimer's β-amyloid plaques[J]. Small, 2020, 16(43): 2002804. https://doi.org/10.1002/smll.202002804.

[16] Lin X, Liu W, Dong X, et al. Epigallocatechin gallate-derived carbonized polymer dots: a multifunctional scavenger targeting Alzheimer's β-amyloid plaques[J]. Acta Biomaterialia, 2023, 157: 524-537. https://doi.org/10.1016/j.actbio.2022.11.063.

[17] Wei Z, Dong X, Sun Y. Quercetin-derived red emission carbon dots: A multifunctional theranostic nano-agent against Alzheimer's β-amyloid fibrillogenesis[J]. Colloids and Surfaces B: Biointerfaces, 2024, 238: 113907. https://doi.org/10.1016/j.colsurfb.2024.113907.

[18] Feng Q, Wang N, Zhang X, et al. Nanoparticle cluster depolymerizes and removes amyloid fibrils for Alzheimer's disease treatment[J]. Nano Today, 2023, 48: 101756. https://doi.org/10.1016/j.nantod.2023.101756.

[19] Geng H, Pan Y, Zhang R, et al. Binding to amyloid-β protein by photothermal blood-brain barrier-penetrating nanoparticles for inhibition and disaggregation of fibrillation[J]. Advanced Functional Materials, 2021, 31(41): 2102953. https://doi.org/10.1002/adfm.202102953.

[20] Wang W, Lin X, Dong X, et al. A multi-target theranostic nano-composite against Alzheimer's disease fabricated by conjugating carbon dots and triple-functionalized human serum albumin[J]. Acta Biomaterialia, 2022, 148: 298-309. https://doi.org/10.1016/j.actbio.2022.06.029.

[21] Shao X, Wang C, Wang C, et al. Novel photocatalytic carbon dots: efficiently inhibiting amyloid aggregation and quickly disaggregating amyloid aggregates[J]. Nanoscale, 2024, 16(16): 8074-8089. https://doi.org/10.1039/D3NR06165E.

[22] Wang Y, Yan C, Qi Y, et al. Harnessing multi-target nanosweepers inhibiting β-amyloid aggregation, scavenging reactive oxygen species and overcoming the blood brain barrier for rescuing Alzheimer's disease[J]. Chemical Engineering Journal, 2025, 508: 161138. https://doi.org/10.1016/j.cej.2025.161138.